Journal of Renewable Energies
Revue des Energies Renouvelables
journal home page : https://revue.cder.dz/index.php/rer

Research Paper

Numerical approach of a fully developed flow in a solar collector adapted to the climate of southwest Algeria

Khelifa Hami [a,*], Abdelkrim Talhi [a] , Belkacem Draoui [b]

[a] *Laboratory of Environmental and Energy Systems LSEE, Institute of Science and Technology, University Center Ali KAFI, Tindouf, Algeria*
[b] *Laboratory of Energetic in Arid Zones, ENERGARID. Faculty of Technology, TAHRI Mohamed University, Béchar, Algeria*

A R T I C L E I N F O

Article history:
Received 06 July 2020
Accepted 29 September 2020

Keywords:
Solar energy
Solar collector
Convection
Turbulence flows

A B S T R A C T

The present work has been conducted with the aim of contributing to the study of heat transfer phenomena in an air solar collector, which deal with transient heat transfer properties and mechanisms. The improvement of heat transfer in the studied system is characterized by the development of the flow between the absorption of cold air and the evacuation of hot air. The equations, which govern the problem dealt with, are those of turbulent and incompressible flows written in Reynolds decomposition for velocity, pressure and temperature, in a mean component and a term of fluctuation, and expressing the conservation of the mass, of the amount of movement and energy. To close the set of transport equations, the turbulence model k-ε was used. We will therefore use this model of turbulence with an improved treatment of wall laws (Enhanced wall treatment), with the intention of solving the laminar sub-layer. The simulation results obtained are valid for temperature values between (30 °C - 50 °C) for heating flows between (200 w / m^2 - 800 w / m^2), the average volume flow obtained is equal to: 0.3 m^3/s. These results are essential for the passive heating of buildings and the drying of agrifood products.

** Corresponding author, E-mail address: hamikhelifa@yahoo.fr*
Tel.: +213 697527407

ISSN: 1112-2242 / EISSN: 2716-8247

1. Introduction

The solar energy is considered one of the most important sources for renewable energy because it is an inexhaustible source. Furthermore, recent studies have confirmed that thirty minute of solar radiation on earth is equal to the world energy request for the whole year. Therefore, solar energy is used in many applications, such as ventilation air preheating, space heating of buildings [1] G. Feng et al., [2] J. F. Belmonte et al., [3] D. Zhao et l., and [4] Hami K. et al, water heaters in homes [5] S. Esakkimuthu et al., [6] C. K. K. Sekyere et al., and [7] M. Mokhtarian et al., then drying agricultural crops [8] R. M. Reddy et al., [9] R. Benrejeb et al., and [10] S. Rezvani et al.

In order to be effective and productive, all the solar energy applications listed above must be integrated with a thermal energy storage unit. The function of a thermal energy storage unit is to absorb and store heat energy. Hence, solar heaters can be operated for a longer period of time during sunset [9] R. Benrejeb et al. Consequently, in recent years, several studies have focused on the development of solar energy systems, particularly the optimal use of solar radiation and the best ways to store solar thermal energy.

Solar energy collectors can also be classified based on their method of work, which can be positive or negative. The positive type uses an electric pump to distribute the heat transfer fluid, while the negative type operates without a pump. Consequently, both types may be used in all types of collectors whether they be flat-plate, evacuated tube or concentrating [10] S. Rezvani et al.

The solar energy collectors can also be grouped into direct or indirect types. A direct type of solar water heating system distributes domestic water during collectors but is inappropriate for frigid atmospheres. The indirect type, on the other hand, is used for heat transfer fluid [11] J. Varghese et al., [12] A. M. Khudhair et al., and [13] A. Shukla et al.

The Evacuated tube collectors differ from other types of collectors due to their vast difference in terms of design and operation are presented by [14] Ali Mohammed Hayder, and [15] N. Mehla and A et al., and .The Evacuated tube collectors mainly consist of glass tubes. Any tube contains two layers: an outer layer made of glass and an inner layer which consists of an absorber plate to solar radiations. The tubes are the main configuration for evacuated tube collectors. Evacuated tube collectors are characterized by their ability to reduce convection and thermal conduction losses due to the space between the tubes, which makes them a heat insulator.

The present work has been conducted with the aim of contributing to the study of heat transfer phenomena in an air solar collector, which deal with transient heat transfer properties and mechanisms. The improvement of heat transfer in the studied system is characterized by the development of the flow between the absorption of cold air and the evacuation of hot air. The equations, which govern the problem dealt with, are those of turbulent and incompressible flows written in Reynolds decomposition for velocity, pressure and temperature, in a mean component and a term of fluctuation, and expressing the conservation of the mass, of the amount of movement and energy. To close the set of transport equations, the turbulence model k-ε was used. We will therefore use this model of turbulence with an improved treatment of wall laws (Enhanced wall treatment), with the intention of solving the laminar sub-layer. The results obtained show a good qualitative and quantitative agreement with that of the literature.

The study of the thermal and dynamic behavior of the area in an air solar collector is the subject of a physical modelling of the phenomenon through the interaction between this system and those climatic conditions (Radiation and ambient temperature) a typical winter period. The heating path of the air mass is shown schematically in Fig. 1.

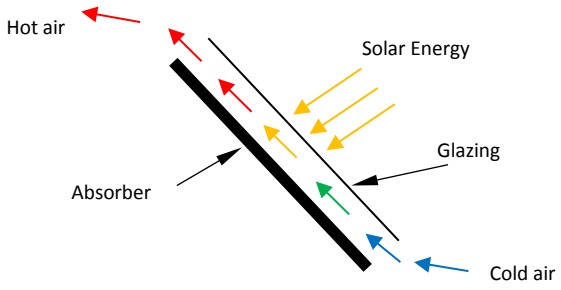

Fig 1. Physical model

In order to obtain a mathematical model for the physical phenomenon studied, we adopt the following assumptions:

- The fluid is Newtonian and incompressible;
- The flow regime is unsteady;
- The physical properties of the fluid are constant except the density obeys the Bossiness approximation in terms of the buoyancy.

2. Mmathematical model

2.1 Equations of the problem

The equations governing the problem addressed are those turbulent incompressible flows and written decaying Reynolds for pressure, speed and temperature with an average component and a fluctuation term, and expressing respectively the mass conservation, momentum and energy:

$$\frac{\partial \bar{u}}{\partial x_i} = 0 \tag{1}$$

$$\frac{\partial \bar{u}}{\partial t} + \bar{u}_j \cdot \frac{\partial \overline{u_i}}{\partial x_j} = -\frac{1}{\rho} \cdot \frac{\partial \bar{P}}{\partial x_i} + \frac{\partial}{\partial x_j}\left[\nu \cdot \left(\frac{\partial \overline{u_i}}{\partial x_j} + \frac{\partial \overline{u_j}}{\partial x_i} \right) - \overline{u_i' u_j'} \right] + \bar{f}_i \tag{2}$$

$$\frac{\partial \bar{T}}{\partial t} + \bar{u}_i \cdot \frac{\partial \bar{T}}{\partial x_i} = \frac{\partial}{\partial x_i}\left[\alpha \cdot \frac{\partial \bar{T}}{\partial x_i} - \overline{u_i T'} \right] \tag{3}$$

i and *j*: represent the direction of flow.

The Reynolds stresses and heat turbulent flows respectively appear in the equations (2) and (3) are expressed in terms of dynamic and thermal fields means as follows [16] P. Chassaing:

$$\overline{u_i' u_j'} = \frac{2}{3} \cdot \delta_{ij} \cdot k - \nu_t \cdot \left(\frac{\partial \bar{u}_i}{\partial x_j} + \frac{\partial \overline{u_j}}{\partial x_i} \right) \tag{4}$$

$$\overline{u_i T'} = \frac{\nu_t}{\mathrm{Pr}_t} \cdot \frac{\partial \bar{T}}{\partial x_j} \tag{5}$$

Where: $\nu_t(x_i, t)$ is a turbulent kinematic viscosity.

$$\nu_t = C_\mu \cdot \frac{k^2}{\varepsilon} \tag{6}$$

$$\mathrm{Pr}_t = \frac{\nu_t}{\alpha_t} \approx 0.85 \tag{7}$$

To close the whole transport equations (1), (2) and (3), the turbulence model k-ε, (8) and (9) was used. This model has the advantage of not requiring very large computation times, especially for simple cases such as the one we are studying.

The two-modelled equations of turbulent kinetic energy k and ε dissipation are described by the following transport equations (8) and (9) [17] R. Schiestel, and [18] A. Fourar:

Equation of turbulent kinetic energy:

$$\frac{\partial k}{\partial t}+\bar{u}_j\frac{\partial k}{\partial x_j}=\frac{\partial}{\partial x_j}\left[\left(\nu+\frac{C_\mu\cdot k^2}{\sigma_k\varepsilon}\right)\frac{\partial k}{\partial x_j}\right]+\frac{C_\mu\cdot k^2}{\sigma_k}\left(\frac{\partial\bar{u}_i}{\partial x_j}+\frac{\partial\bar{u}_j}{\partial x_i}\right)\frac{\partial\bar{u}_i}{\partial x_j}-\varepsilon \quad (8)$$

Equation of dissipation:

$$\frac{\partial \varepsilon}{\partial t}+\bar{u}_j\frac{\partial \varepsilon}{\partial x_j}=\frac{\partial}{\partial x_j}\left[\left(\nu+\frac{C_\mu\cdot k^2}{\sigma_\varepsilon\varepsilon}\right)\frac{\partial \varepsilon}{\partial x_j}\right]+C_{\varepsilon 1}\cdot C_\mu\cdot k\cdot\left(\frac{\partial\bar{u}_i}{\partial x_j}+\frac{\partial\bar{u}_j}{\partial x_i}\right)\frac{\partial\bar{u}_i}{\partial x_j}-C_{\varepsilon 2}\cdot\frac{\varepsilon^2}{k} \quad (9)$$

The constants called k-ε model are standards for values:

$$C_\mu=0.09,\ \sigma_k=1,\quad \sigma_\varepsilon=1.22,\quad C_{\varepsilon 1}=1.44,\quad C_{\varepsilon 2}=1.9$$

Transport equations (1), (2), (3), (8) and (9) are discretized by the method of the control volumes, and resolved by the simple algorithm [20] S. V. Patankar. In order to achieve a compromise between the computation time and accuracy of simulation results, an optimization study was made of the influence of no space and time (Courant-Friedrichs-Lewy (1928) or CFL condition. It is necessary and sufficient for stability) [21] K. Abe et al., and [22] L. T. Wong et al. It is estimated that convergence is reached when the relative differences in all variables calculated at various nodes of the mesh Fig. 3, fall below (R = 10^{-4}) between two successive iterations.

2.2 Initial and boundary conditions

At: t = 0 $\quad u=v=w=k=\varepsilon=0$ and $\quad T=T_i=6$ °C

- Condition of adherence to the walls (u, v, w) = (0,0,0);
- The contest between the absorber (*ab*) and air (*f*) is assumed to be perfect in the air space;

So : $-\lambda_{ab}\frac{\partial T_{ab}}{\partial y}=-\lambda_f\frac{\partial T_f}{\partial y}=\phi_s$ and $T_{ab}(y)=T_f(y)$ (interface)

- The estimated global solar radiation is expressed by the model of LUI&JORDAN [19]:

$$\varphi_s=S^*+D_i^*\ ;\ i=45°\ ; \quad (10)$$

$$S^*=I^*\times\left[\sqrt{2}/2\times\cos(h)\times\cos(a-\gamma)+\sqrt{2}/2-\sin(h)\right]; \quad (11)$$

$$D_i^*=\left[\frac{1+\sqrt{2}/2}{2}\right]\times D_h^*+\left[\frac{1-\sqrt{2}/2}{2}\right]\times a^*\times G_h^* \quad (12)$$

$$D_h^* = G_h^* - I^* \times \sin(h). \quad (13)$$

With:

The value of solar radiation "I^*", received by a surface perpendicular to the solar rays placed at the upper limit of the Earth's atmosphere varies during the year with the Earth / Sun distance. Its average value "I^0" called solar constant is of the order of 1354 ($w.m^{-2}$). As a first approximation, we can calculate the value of "I^*" according to the number of the day of the year "nj" by the following relation:

$$I^* = I_0 x[1+ 0.033 \times \cos (0.984 \times nj)] \quad (14)$$

The height of the sun (h): The height of the sun is the angle formed by the direction of the sun and its projection on the horizontal plane. It is particularly equal to 0 ° at astronomical sunrise and sunset; its value is maximum at noon, in true solar time. The expression for the height of the sun is given by:

$$\text{Sin (h)} = \sin(\varphi).\sin(\delta) + \cos(\varphi).\cos(\delta)\cos(\omega) \quad (15)$$

φ : Latitude;

δ: The declination of the sun;

ω: The hour angle.

For the present work, the geographic data are:

- Latitude = 31 ° 62 'N,
- Longitude = -2 ° 23 'W,
- Altitude = 773m,
- Albedo (a*) = 0.2.

The azimuth (a): This is the angle between the projection of the direction of the sun on the horizontal plane and the south. The azimuth is counted positively towards the west and negatively towards the east. The following relation gives it:

$$\text{Sin(a)} = \frac{\cos(\delta).\sin(\omega)}{\cos(h)} \quad (16)$$

The declination (δ): this is the angle made by the plane of the equator with that of the ecliptic. It varies during the year from + 23°27' to - 23°27' and determines the inequality of the lengths of the days; it is equal to 0 at the equinoxes. δ is given by the following relation :

$$\delta = 23.45° \text{ Sin}\left(\frac{360}{365} \times (284 + j)\right) \quad (17)$$

j: The number of the day in the year counted from January 1st.

The hour angle (ω): This is the angle between the original meridian passing through the south and the projection of the sun on the equatorial plane, it measures the course of the sun in the sky. The following relation gives it:

$$\omega = 15\ (TSV - 12) \tag{18}$$

TSV: true solar time

It is 0 ° at solar noon, then each hour corresponds to a variation of 15 °, because the period of the earth in its rotation on itself is equal to 24 hours. Counted negatively in the morning when the sun is east and positively in the evening.

True solar time, at a given instant and location, is the hour angle of the sun ω. It is given in the following form:

$$TSV = 12 + \frac{\omega}{15} \tag{19}$$

The mean solar time is sometimes called local time; the following relation gives it:

$$TSM = TSV - Et \tag{20}$$

$$Et = 9.87 \sin\left[2.\frac{360}{365}(N-81)\right] - 7.53 \cos\left[\frac{360}{365}(N-81)\right] - 1.5 \sin\left[\frac{360}{365}(N-81)\right] \tag{21}$$

- Et: is the equation of time expressed in minutes.
- N: is the number of the day in the year.

The set of equations of this model was presented in a text file in the form of a computer program in language (C++) for adaptation as a boundary condition at the interface of the software of the calculator using the extension of the coupling (user defined function UDF).

The following flowchart (Fig 2) summarizes the steps in solving this study:

- τ: represents the step of the iterative calculation;
- τ = 0: initialization of the calculation;
- (τ+1): next step of the iterative calculation.

The convergence test chosen for this simulation is: $R \geq 10^{-4}$ (weighted residue).

The stop test of the chosen calculation for this simulation is: $\tau \leq 86400$ (s) (the time needed to simulate a typical day).

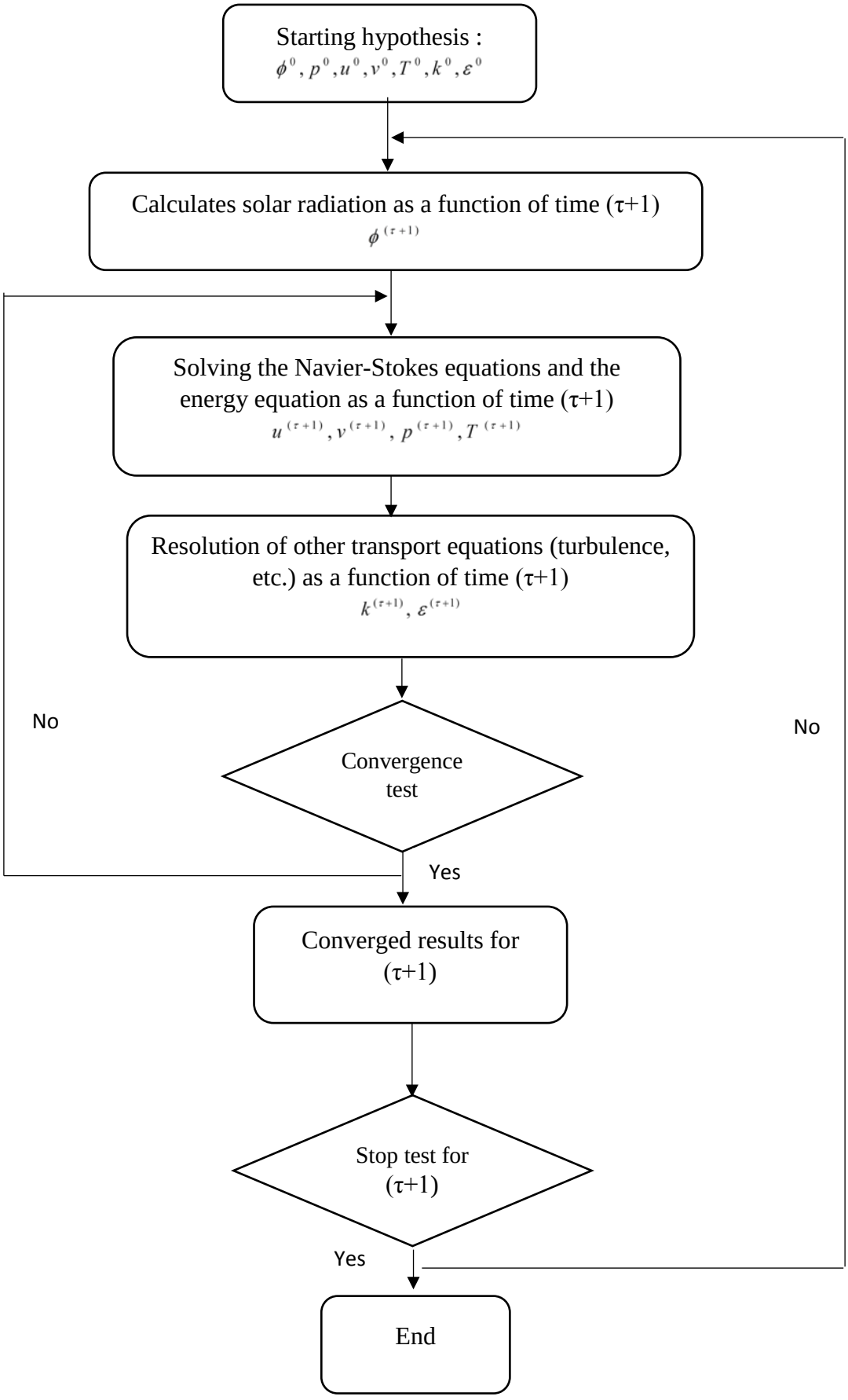

Fig 2. The flowchart of the present work

3. Results and discussion

In order to verify that our computation "holds well the road", it is important to have y+ of the order of (y+ ~1). However, a larger value is acceptable as long as it remains in the viscous sub-layer (y^+ 4 or 5) [23] N. Marzouqy. The following results (Fig 3) confirm that we are in this range. Note that we had to make an adaptation of the mesh to decrease the values of y + since our mesh was not close enough near the walls. This is done in the fluent menu (Adapt Yplus / Ystar).

The following relations (22, 23 and 24) expresses the values of y+ near the hot wall and the cold wall:

$$y^+ = \frac{y \cdot u^*}{\nu} \tag{22}$$

$$u^* = \sqrt{\tau_{ab} / \rho} \tag{23}$$

$$\tau_{ab} = \mu \left(\frac{\partial u}{\partial y} \right)_{ab} \tag{24}$$

The history of the convergence of the air inlet and outlet velocity of the solar collector is shown in Fig 4. There are two phases, the first represents the transient phase due to the unstable initial state of the system, and the second is a stable phase represents the inertial state of this system.

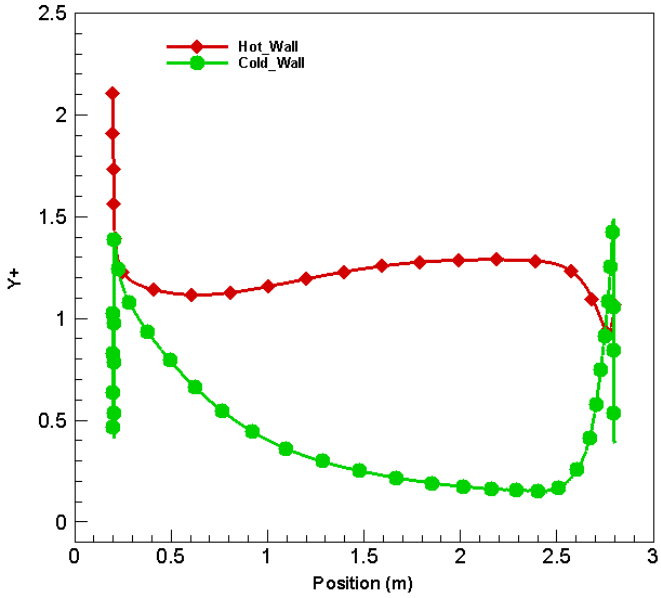

Fig 3. Test of mashes quality

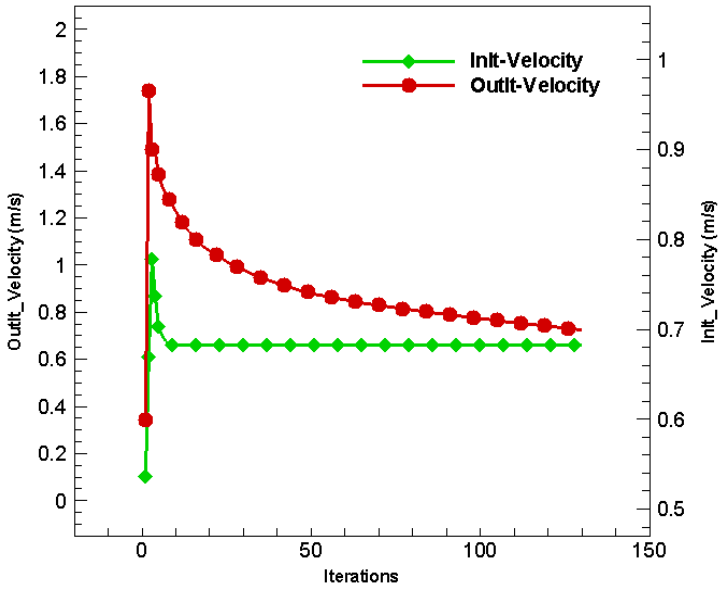

Fig 4. Test of convergence

The average Nulsset values depending on local Grashof literature are compared in this study (Table 1). These results are in good agreement in general, the values obtained by Ferris [24] are the closest to the results of this work or the error does not exceed 5%.

Table 1. Validation: Nulsset for different correlations of literatures [24].

Case studies	Nulsset (Nu)					
	Grashof (G_r)	10^7	10^8	10^9	10^{10}	Error (%)
Ferris		25.32	54.13	115.72	247.41	1.61
Cibs		24.30	51.95	111.10	237.44	2.52
Arharae		23.90	51.07	109.19	233.45	4.27
Present work		24.91	53.26	113.86	243.42	-

In Fig 5 are shown the solar radiation reading and the temperature curve on the surface of the absorber during a typical sunny day. The maximum value obtained by this simulation is 60.275 (° C) at 13.00 H for an incident solar radiation, which is equal to 812.930 (w / m^2).

Fig 6 shows the resulting velocity field in the direction of flow, where it is clear that the flow is strongly accelerated at the hot zone. By the effect of the viscosity at the level of the manifold, the speed values are between low ambient values at the inlet and maximum ones at the outlet of the system.

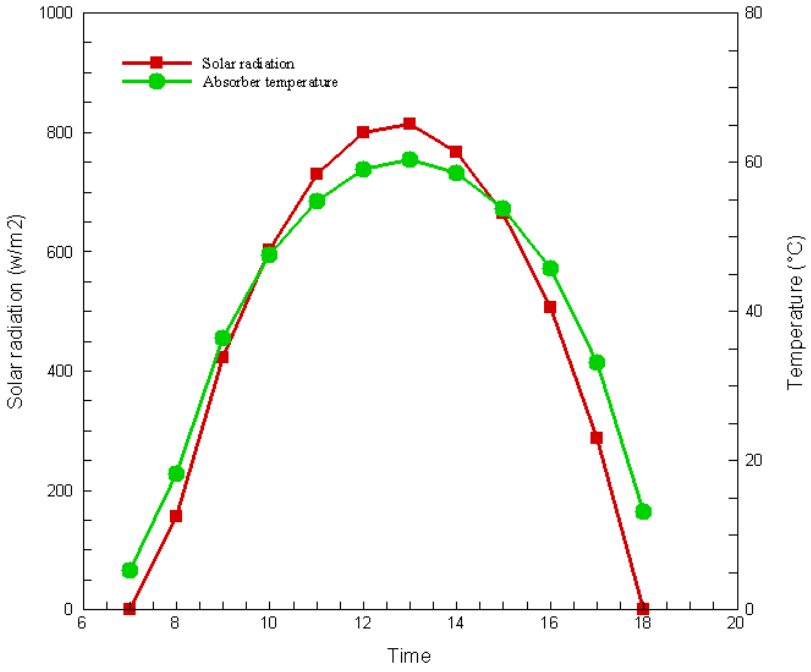

Fig 5. Solar radiation ant absorber temperature during the period of sunshine

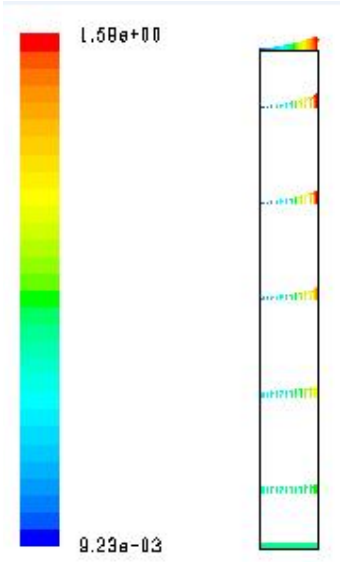

Fig 6. Resulting velocity field

The evolution of the local Grashof number along the hot wall are presented in Fig 7. We notice a change in the flow regime at the hot boundary layer. The results obtained showed that for G_{rh} $4x10^8$ the flow regime is certain laminar with (h 0.46m), while for $G_{rh} > 10^9$ the flow regime becomes turbulent with (h> 0.6m). For the transient zone (0.46m < h < 0.6m).This change in diet is characterized by increased convective transfer. The near the absorber, region serves as a motor to flow, substantially all of the injected energy to the thermal wall remains confined in this region and serves to accelerate the fluid. The neutral zone (laminating zone), is driven by the near absorber region and decelerated with the height retention rate. Competition settles then

between the heating wall, which tends to increase shear and turbulent mixing, created by shear, which tends to equalize the flow and thus reducing the shear. When this turbulent mixture becomes significant enough, a flow regime change occurs, it is the mixing zone. In this zone, located after the transition, the flow is mixed, homogenized by turbulent mixing, shear decreases and the channel center is warming. Velocity fluctuations are no longer fed by the shearing but directly from the turbulent flow of heat. Indeed, an analysis of the terms of production of turbulent kinetic energy shows a competition between the production of viscous origin, which dominates in channel input and that of thermal origin, which grows before the transition and after dominates.

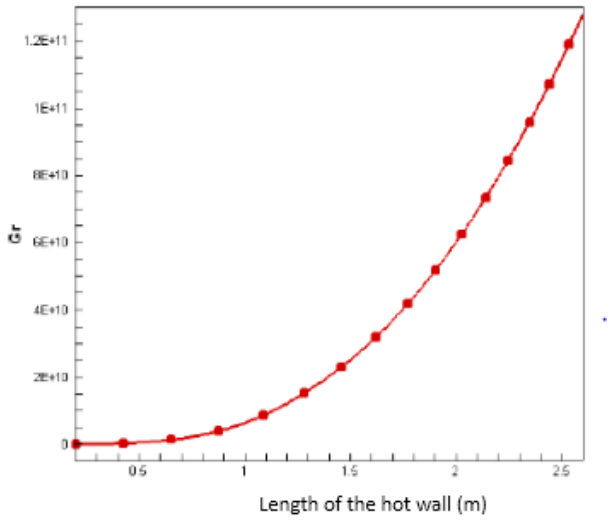

Fig 7. Values of the local Grashof number along the hot wall, for ϕ_s = 800 (w / m^2)

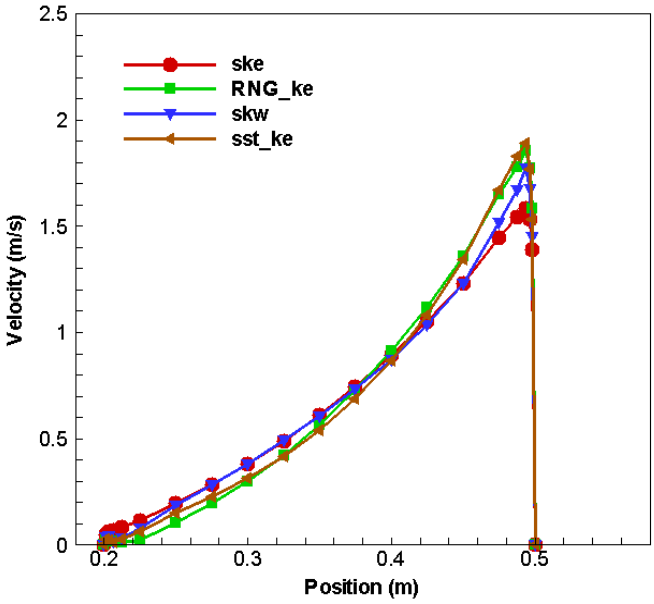

Fig 8. Velocity profile vs Turbulences models

The turbulence model k-ε was used in this study to close the set of basic equations. Fig 8 and 9 represent a comparison between this model and others in the literature to assert the feasibility of this choice. The superimposition of velocities and temperatures shows a good agreement between all the models that we simulated, this confirms that our calculation will have the right way of point of view of the mathematical and physical modelling.

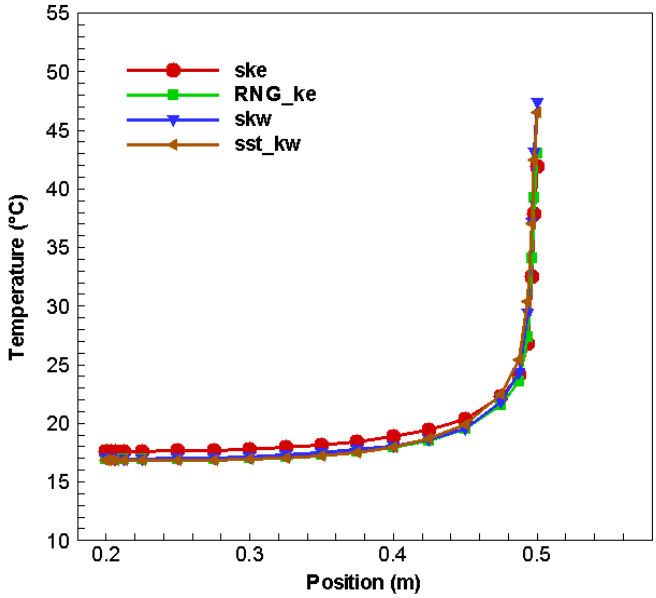

Fig 9. Temperature profile vs Turbulences models

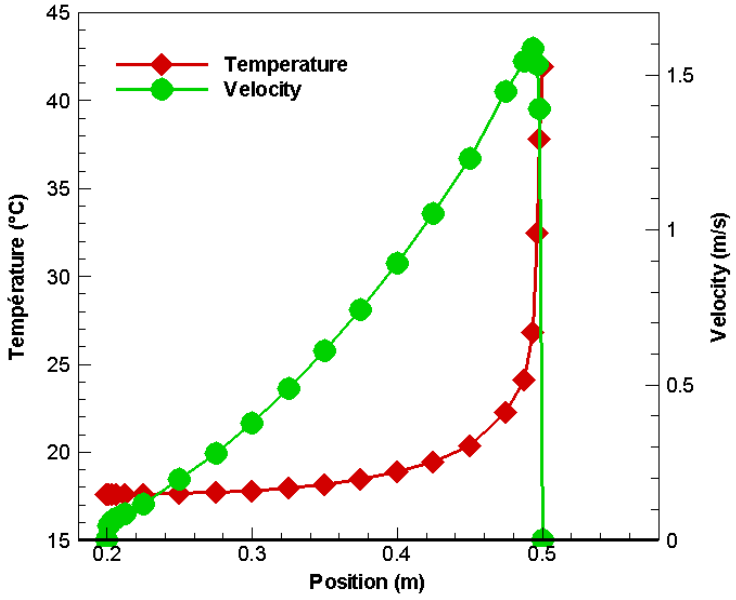

Fig 10. Dynamic ant thermal boundary layer

In the neighborhood of the hot surface, develop the dynamic and thermal limit layers, in whom we observe the variations of the velocity and the temperature. The superimposing of the profiles of temperature and the vertical component of velocity, given to the Fig 10, in the quotation y = 1.50 m, shows that the thermal limit layer is 3 times less thick than the dynamic limit layer. This big difference is not certainly an effect attributed to the viscosity of the air. It is not probably either due to the inverse flow of border of limit layer, which passes by the temperature of the glazing. There is a homogenization of the temperature in the external zone of the dynamic limit layer because of the turbulent brewing.

This section is to describe the changes in the different velocity profiles and temperature, depending on the height of the hot and cold wall. Developments different velocity's and temperature profiles, depending on the sunlight hours in (100 W/m^2 – 800 W/m^2). It is based on the numerical results, during which the simulations were made near the hot and cold wall, are shown in Fig 11 and 12.

The study of flow near the walls represented in Fig 11 and 12, are necessary for the determination of heat transfer by convection between the wall and the air around it. Away from the hot surface, air at an average velocity V_m and an average temperature T_m. In the immediate vicinity of the surface, the air temperature is very close to that of the surface. The air velocity is almost zero.

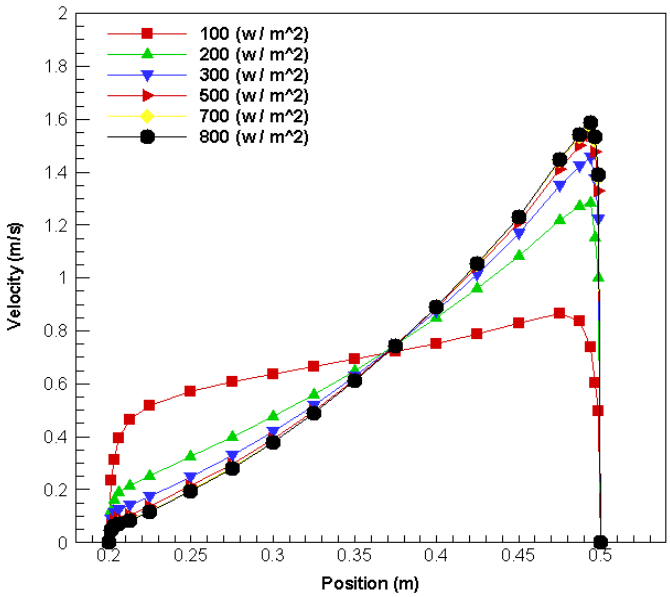

Fig 11. Velocity profiles vs. solar energy

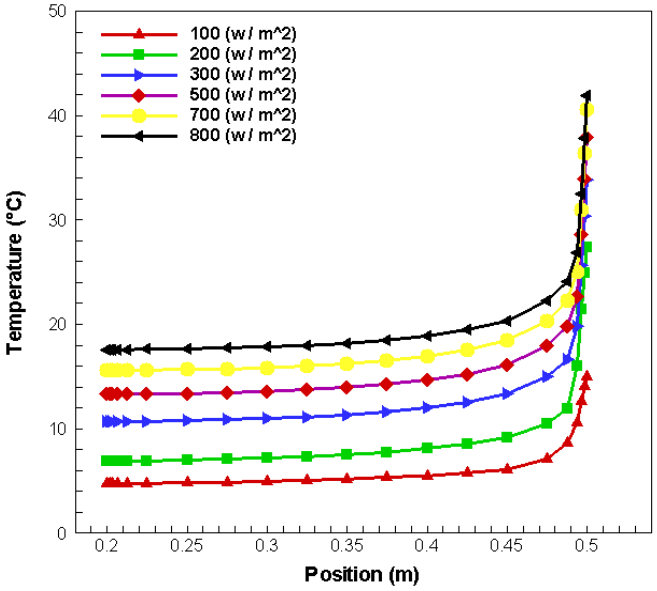

Fig 12. Temperature profiles vs. solar energy

4. Conclusions

The simulation results shown in this work, they allow the presentation and exploitation of results obtained from simulations in 2D. They were made with a heating, condition due to sunlight. The velocity profiles and the average temperature were presented and analyzed. The study of these profiles based on the height in the solar collector has helped to identify a flow regime change. The simulation results obtained are valid for temperature values between (30 °C - 50 °C) for heating flows between (200 w / m^2 - 800 w /m^2), the average volume flow obtained is equal to: 0.3 m^3/s. These results are essential for the passive heating of buildings and the drying of agrifood products.

Nomenclature

D^*	diffuse solar flux (w/m²)
S^*	direct solar flux (w/m²)
f_i	volume forces (kg.m s^{-2})
k	turbulent kinetic energy (m^2 .s^{-2})
p	pressure (Pa)
P'_i	pressure fluctuation (Pa)
$\overline{P}$	average pressure (Pa)
T_{ab}	absorber temperature (°C)
T_f	air temperature (°C)
T'_i	temperature fluctuation (°C)
$\overline{T}$	average temperature (°C)
u_i	velocity component (m.s^{-1})
u'_i	velocity fluctuation component (m.s^{-1})
u^+	boundary layer velocity
u_τ	characteristic friction velocity
y^+	distance to the wall

Greek symbols

ρ	density (kg/m^3)
α	thermal diffusivity (m^2 .s^{-1})

α_t	turbulent thermal diffusivity ($m^2 .s^{-1}$)	φ_S	heat flux (w/m^2)
		τ_w	shear stress
ε	dissipation rate of the turbulent kinetic energy	μ	dynamic viscosity ($m^2 .s^{-2}$)
		ν	kinematic viscosity ($m^2 .s^{-2}$)

5. References

[1] G. Feng et al., "Thermal storage exchanger based on phase change material applying to solar fresh air system", Mater. Res. Innov. 2015.

[2] J. F. Belmonte, M. A. Izquierdo-Barrientos, A. E. Molina and J. A. Almendros-Ibez, "Air-based solar systems for building heating with PCM fluidized bed energy storage", Energy Build. pp. 150-165, 2016.

[3] D. Zhao, J. Ji, H. Yu, W. Wei and H. Zheng, "Numerical and experimental study of a combined solar Chinese kang and solar air heating system based on Qinghai demonstration building", Energy Build, 2017.

[4] K. Hami et al., "Modélisation d'un système de chauffage passif dans la région de Béchar", Revue des Energies Renouvelables Vol. 13(2), pp. 355 – 368, 2010.

[5] S. Esakkimuthu, A. H. Hassabou, C. Palaniappan, M. Spinnler, J. Blumenberg, and R. Velraj, "Experimental investigation on phase change material based thermal storage system for solar air heating applications", Sol. Energy, Vol. 88, pp. 144-153, 2013.

[6] C. K. K. Sekyere, F. K. Forson and F. W. Adam, "Experimental investigation of the drying characteristics of a mixed mode natural convection solar crop dryer with back up heater", Renew. Energy, pp. 532-542, 2016.

[7] M. Mokhtarian, H. Tavakolipour and A. Kalbasi Ashtari, "Effects of solar drying along with air recycling system on physicochemical and sensory properties of dehydrated pistachio nuts", LWT – Food Sci. Technol, pp. 202-209, 2017.

[8] R. M. Reddy, N. Nallusamy, and K. H. Reddy, "Experimental Studies on Phase Change Material-Based Thermal Energy Storage System for Solar Water Heating Applications. J. Fundam", Renew. Energy Appl, pp. 1-6, 2012.

[9] R. Benrejeb, O. Helal, and B. Chaouachi, "Study of the effect of truncation on the optical and thermal performances of an ICS solar water heater system", Sol. Energy, Vol. 132, pp. 84-95, 2016.

[10] S. Rezvani, P. A. Bahri, T. Urmee, G. F. Baverstock and A. D. Moore, “Techno-economic and reliability assessment of solar water heaters in Australia based on Monte Carlo analysis”, Renew. Energy, Vol. 105, pp. 774-785, 2017.

[11] J. Varghese, Samsher and K. Manjunath, “A parametric study of a concentrating integral storage solar water heater for domestic uses”, Appl. Therm. Eng, Vol. 111, pp. 734-744, 2017.

[12] A. M. Khudhair and M. M. Farid, “A review on energy conservation in building applications with thermal storage by latent heat using phase change materials”, Vol. 45, pp. 263-275, 2004.

[13] A. Shukla, D. Buddhi and R. L. Sawhney, “Solar water heaters with phase change material thermal energy storage medium: A review”, Renew. Sustain, Energy Rev, Vol. 13, pp. 2119-2125, 2009.

[14] Ali Mohammed Hayder, Azwan Bin Sapit and Qahtan Adnan Abed, “Review of solar thermal storage techniques, ARPN Journal of Engineering and Applied Sciences”, Vol. 12, pp. 6103-6119, 2017.

[15] N. Mehla and A. Yadav, “Experimental analysis of thermal performance of evacuated tube solar air collector with phase change material for sunshine and off-sunshine hours”, Int. J. Ambient Energy, Vol. 750, pp. 1-16, 2015.

[16] P. Chassaing, “Turbulence en mécanique des fluides : Analyse du phénomène en vue de sa modélisation à l’usage de l’ingénieur”, Polytech, Cepadues, 2000.

[17] R. Schiestel, “Les écoulements turbulents : Modélisation et simulation, 2nd ed. Hermes”, 1998.

[18] A. Fourar, O. Timizar, and F. Abdessemed, “Contribution à l’etude d’un écoulement turbulent dans une conduite. Développement de la couche limite turbulente“, Science Lib Editions Mersenne, Vol. 3, No. 110302, 2011.

[19] K. Hami et al., “Thermal fluid modeling of a passive heating system”, Renewable and Sustainable Energy, AIP Publishing, Vol. 8, No. 013113, 2016.

[20] S. V. Patankar, “Numerical Heat Transfer and Fluid Flow”, McGraw-Hill, Washington, Etats-Unis, 1980.

[21] K. Abe, N. Higashimori, M. Kubo, and Y. Iso, “A remark on the Courant-Friedrichs-Lewy Condition in finite difference approach to PDE’s”, Adv. Appl. Mathematics Mechanics, Vol. 6, pp. 693–698, 2014.

[22] L. T. Wong and W. K. Chow, “Solar radiation model”, Appl. Energy, Volume 69, pp. 191–224, 2001.

[23] N. Marzouqy, “Cours Mécanique des Fluides, Université des Mines”, 2006.

[24] A. Trombe et al., “Use of inverse method of determine natural convection heat transfer coefficients in unsteady state”, journal of heat transfer, pp.1017-1026, 2003.